Experimental and theoretical investigations into structural, morphological and optical characters of the Al_2O_3, CuO and ZnO-based nanofluids for interfacial tension reduction

M. Usman [a], Arhum [a], M. A. Zaidi [a], N. Nasir [a], B. Tanveer [c], S. A. Cheema [a], A. Rehman [b], Z. Tanveer [a,*]

[a] *Department of Applied Sciences, School of Science, National Textile University Faisalabad, Pakistan.*

[b] *Department of Textile Engineering, School of Engineering and Technology, National Textile University Faisalabad, Pakistan.*

[c] *Department of Biochemistry, Government College University Faisalabad, Pakistan.*

This research elucidates interfacial tension behavior of nanofluid of Al_2O_3, CuO and ZnO. The synthesis was facilitated by sol gel method. The features are elaborated by employing SEM, XRD and RAMAN. The soft of CASTEP Material studio was considered to simulate energy band gap, partial density of states and dielectric constant. The interfacial tension analysis was conducted by placing crude oil. The outcomes reveal that dielectric behaviour along with interfacial tension significantly varies across the nanofluids. The extravagant performance of ZnO-based nanofluid is witnessed in comparison to other contemporaries. This extent of decrement remained 11.3% using ZnO-based nanofluid.

(Received November 28, 2024; Accepted February 25, 2025)

Keywords: Metal-based nanosuspension, Interfacial tension analysis, Dielectric behavior, Density of states, Energy band gap

1. Introduction

The current era of smart technologies is witnessing aggressive and unprecedented upsurge in the energy consumption [1]. More alarmingly, according to a conservative estimation the energy demand is projected to rise 50% till the end of year 2030 [2]. The attainment of sustainable growth is thus coinciding with diminish of existing natural energy resources. The urge of conversion of available resources into reserves swiftly results in finding the pathways leading towards more efficient use of existing resources [3]. The emergence of nanotechnologies is unfolding novel solutions of the multifaceted complexity of optimization of reservoir engineering operations [4]. These cutting-edge advancements are found to delineate the resolves of the issue by offering elegant manipulation of materials and devices at design level. Owing to the exceptional characters such as, exaggerated volume to surface ratio, delicately stable dispersion and elevated reduction of interfacial tension (IFT), nanoparticles are playing celebrated role in this regard [5]. The emerging literature of multi-disciplinary orientation well cherishes the utility of nanoparticles especially in the field of reservoir engineering. For example, [6] reported the stream of usages of Silica nanoparticles to attain convincingly stable oil-in-water emulsion with respect to varying polymer chain grafting densities. Further, [7] argued notable reduction in IFT of Kerosene-water resulting from the launch of hybrid nanoparticles of Multiwall Carbon nanotubes and Silicon Oxide. Furthermore, [8] advocated the employment of Fe_2O_3-SiO_2 to reduce the IFT by the alteration of contact angle. The more recently produced research literature firmly focuses on variety of application in reservoir operations such as, proficient oil recovery [9-12], chemical and water flooding, wettability alteration, drilling [13-17].

* Corresponding author: zaighumtanveer@yahoo.com
https://doi.org/10.15251/DJNB.2025.201.213

This research provides elaborative account of investigating Al_2O_3, CuO and ZnO as potential sweeping agent to reduce the IFT between oil-rock interfaces. It is noteworthy that one of the desirable delicacies of reservoir operations is to maintain the electro-neutrality of the solid – liquid interface [18]. Therefore, the dielectric characters of nanomaterials to be used become a matter of prime interest. One may notice that the choice of above documented nanomaterials offers an elaborative extent of flexibility in this regard. The consideration of Al_2O_3, CuO and ZnO in single study enables the investigator to incorporate different structural formations such as trigonal, monoclinic and hexagonal structures, respectively. Other than these attractions, the focused interesting materials are widely appreciated due to fascinating physicochemical properties [19-23]. For example, there is no dearth of literature appreciating Al_2O_3 for elegancies such as, high-electric-constant [24], low deposition temperature [25], excellent surface topology [26] and attractive thermodynamic stability [27]. One may notice stream of applications encapsulating wide range of multidisciplinary executions such as, smart system communications, environment robust energy devices and energy storage and communication devices [28-30]. Similarly, CuO is known for characteristics such as, high surface reactivity, chemical stability, and strong photo-catalyst properties [31, 32]. The applicability of the material and its derivatives can be seen in fields such as, industrial catalyst, gas sensor, and environmental remediation [33]. Lastly, the rightly grossed fame of ZnO is rooted in delicacies such as, exciting exciton binding energy, attractive electron mobility and direct wide band gap. The aforementioned subtleties earned unique places for all three considered materials in diverse fields of scientific inquiries spanning over health surveillance, smart energy conversion hardware, industrial and military applications [34-38].

The meet of objectives is facilitated by the launch of keen investigation on two major frontiers that is (i) – experimental synthesis and characterizations of the considered nanoparticles and (ii) – simulation-based evaluation of optimal nanostructure mimicking reservoir environment.

This article is mainly divided into five sub-parts. The synthesis and simulation settings are elaborated in section 2. Whereas, section 3 comprehends the results of the investigations. The section 4 is dedicated to the discussions of the outcomes. Lastly, section 5 concludes the research by summarizing main findings along with few future research potentials.

2. Experimental (synthesis and simulation)

2.1. Synthesis of nanomaterials

The considered nanoparticles are synthesized by the employment of sol-gel method. For the synthesis of Al_2O_3 nanoparticles 18.75g of aluminum nitrate nanohydrate, $Al(NO_3)_2.9H_2O$, is completely dissolved in 100 mL of pure water. This was further stirred for 550 rpm at room temperature in a fume hood. The 28g of aluminum isopropoxide, $Al(O\text{-}i\text{-}Pr)_3$, is added into the solution. After that 5ml of 2-ethilenglycole is added drop by drop into the solution for three hour at temperature maintained at 80 °C. This heating process resulted in a thick and sticky gel. The product was then rested for drying process for five hours at 80 °C temperature constituting the yellowish solid formation. The final product was crushed until the attainment of fine powder form. Finally, the powder is annealed at 1000 °C for 4 hours using a furnace. Al_2O_3 nanofluid of 0.05 wt% is prepared by dispersing 0.5g of Al_2O_3 nanoparticle in 1L of 30,000 ppm brine. The nanofluid is then placed into an ultrasonic bath for 2 hours to achieve homogeneous suspension in the base fluid. Further, the synthesis of CuO nanoparticles is also facilitated through sol-gel route. The objectives were instigated by dissolving 10g of Cu $(NO_3)_2.3H_2O$ into 40 ml of ethyl alcohol. The homogeneous solution was achieved by heating at 70 ºC while stirring at 300 RPM in a fume hood for one hour. This exercise resulted in the production of light green gel. The sample was then moved to the oven for drying at 120 ºC for 14 hours. Next, the sample was crushed into a fine powder before annealing where annealing temperature was set at 500 ºC for 1 hour. Lastly, for ZnO preparation, Zinc acetate (2 moles), and sodium hydroxide (1 mole) pellet (in deionized water) was dissolved in 100 mL of isopropyl alcohol. The solution was stirred using magnetic stirrer at room temperature. Ammonia solution was added drop wise, and the solution was stirred again for 3 hours at room temperature. Then the solution is filtered and washed with deionized water before drying at 50 °C for an hour. The form dried gel calcined at 200 °C for four hours by using a muffle furnace.

2.2. Simulation setup

The proceedings of this research are facilitated by mimicking wide range of experimental states especially focusing the harsh environment. The simulations of the material loadings are conducted by the employment of the soft of CASTEP Material studio. The nanoparticles of Al_2O_3, CuO and ZnO are mimicked by using 144, 68 and 36 electron per unit cells, respectively. Further, the energy band gap comparison of the considered dielectric nanomaterials was persuaded at 2.2 eV for Al_2O_3, 1.2 eV for CuO, and 0.78 eV for ZnO.

3. Results

3.1. Characterizations

3.1.1. X-ray diffraction (XRD)

The crystallinity of the prepared nanomaterials is documented by employing the XRD technique. The figure 1 (a, b and c) depicts the X-ray analysis patterns in the illustration of the crystallographic structure of Al_2O_3 (Figure 1(a)), CuO (Figure 1(b)) and ZnO (Figure 1(c)) nanomaterials while annealing at 1000°C for 4 hours. The major peaks of Al_2O_3 correspond to the (1 0 4) and (1 1 3) plane of a trigonal system (hexagonal axes). The average crystallite size of the Al_2O_3 nanoparticle is estimated as 43.95nm by using Debye-Scherer formula. Moreover, XRD results showed a formation of CuO nanoparticles with monoclinic structure. The XRD spectra exhibited two main peaks at 35.58^o and 38.77^o corresponding the planes (1 1 -1) and (1 1 1). The average crystallite size of the CuO nanoparticle was calculated to be 36.92nm. Lastly, the X-Ray diffraction pattern of ZnO is focused. The prominent peaks are witnessed at the plane (1 0 1), (2 0 0) and (1 0 0), corresponding to the standard structure of zinc oxide phase. Whereas the average particle size of 25.2 nm is calculated.

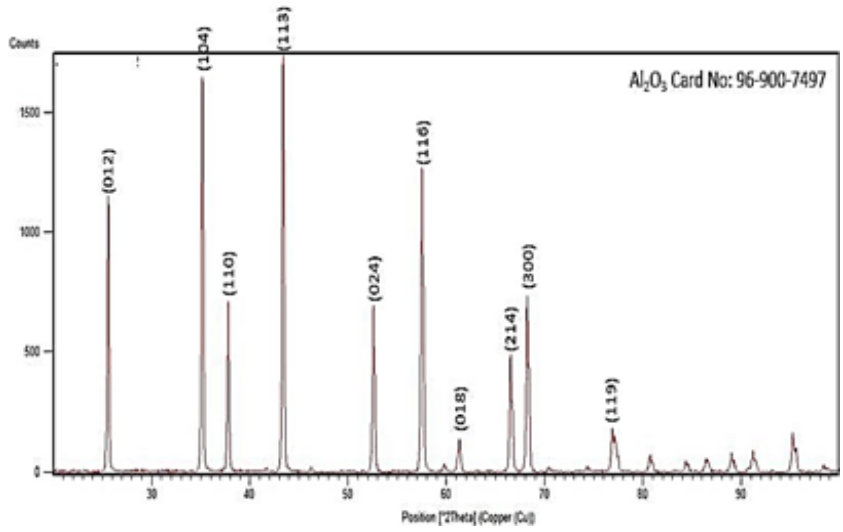

Fig. 1 (a). XRD analysis for Al_2O_3-based nano-material.

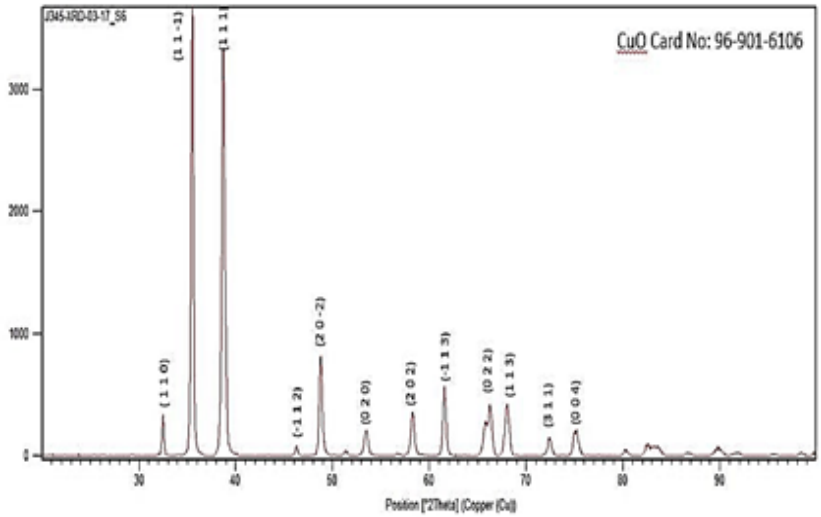

Fig. 1 (b). XRD analysis for CuO-based nano-material.

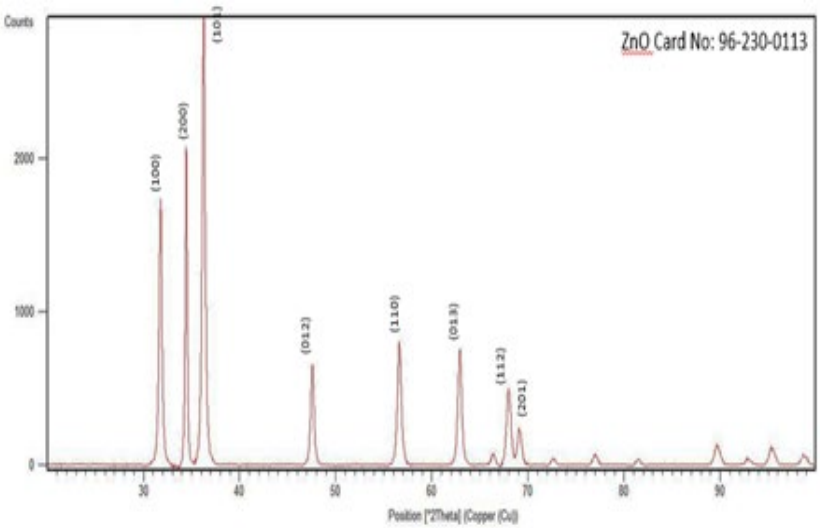

Fig. 1 (c) XRD analysis for ZnO-based nano-material.

3.1.2. Scanning electron microscope (SEM)

The morphological features of the prepared nanomaterials are investigated by the launch of SEM analysis. The figure 2 (a, b and c) does the job of compiling the SEM images. The SEM analysis substantiated the realization that Al_2O_3 samples have grain sizes in the range of 66.78 nm to 127.7 nm ((Figure 2(a))). The particle size of CuO is found to be ranging from 63.47nm to 82.35nm. Further, agglomeration of CuO (Figure 2(b)) nanoparticles was observed which is anticipated to be the result of the togetherness of powder sample stuck due to the effect of surface tension. Lastly, SEM images of ZnO reveals that the particle size ranges from 31.34 nm to 54.01 nm (Figure 2(c)). Also, the agglomeration of ZnO nanoparticles is vividly observed resulting the small particles agglomerate together and thus forming a large cluster.

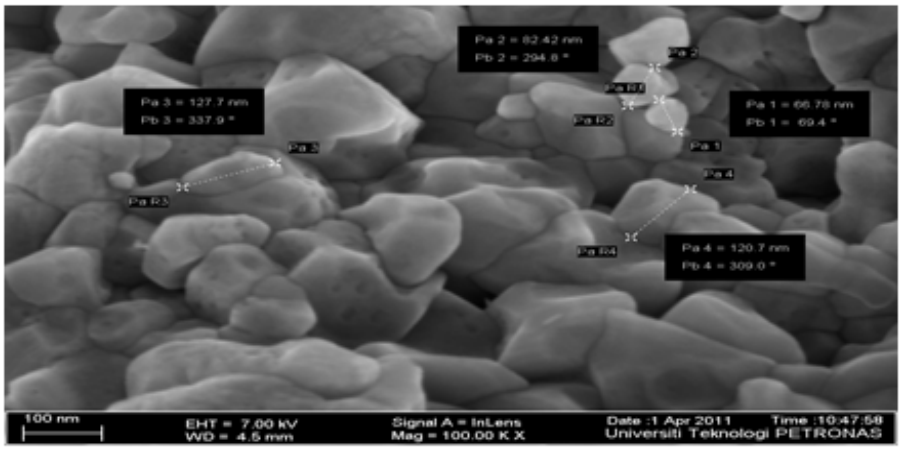

Fig. 2 (a). SEM imagery for Al_2O_3-based nano-material.

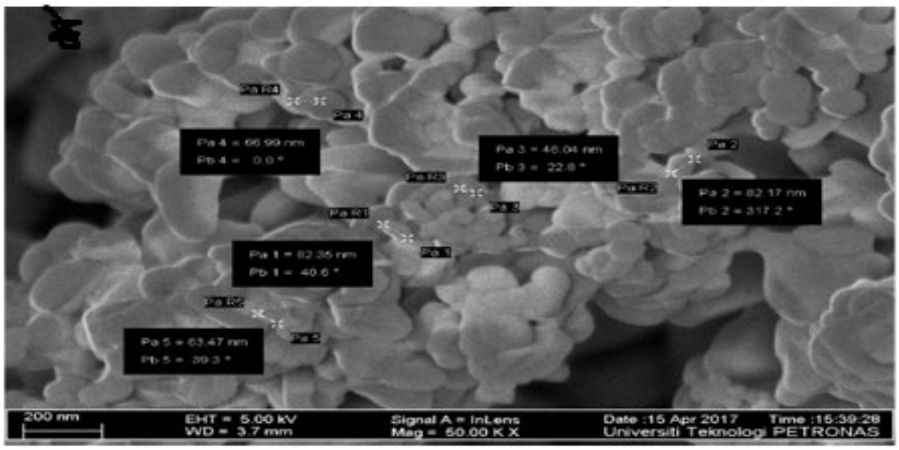

Fig. 2 (b) SEM imagery for CuO-based nano-material.

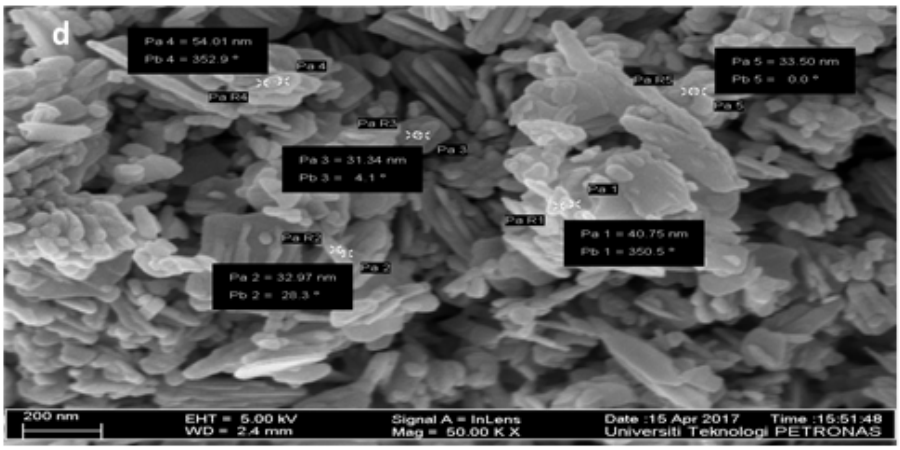

Fig. 2 (c). SEM imagery for ZnO-based nano-material.

3.1.3. RAMAN spectroscopy

The wide range of RAMAN spectrum of Al_2O_3, CuO and ZnO-based nanoparticles grown through sol gel technique at room temperature are studied. Figure 3 presents the display of the

outcomes of the investigation. For the sample Al_2O_3, strong RAMAN spectrum was observed around 462 cm^{-1} due the pure concentration of Al_2O_3. Also, few small peaks around 300 cm^{-1}, 386 cm^{-1}, 421 cm^{-1}, 614 cm^{-1}, 651 cm^{-1}, 752 cm^{-1}, and at 994 cm^{-1} are observed through the spectrum. This is consistent with the existing literature. Next, the RAMAN patterns of CuO-based nanoparticles reveals the existence of six peaks of CuO. The more obvious RAMAN peak of CuO with sharp intensity appeared at 465 cm^{-1} indicating the fundamental behavior of CuO. Moreover, a broad hump around 268 cm^{-1} was also witnessed due to secondary phases. There are also few small peaks of CuO exhibited at 299 cm^{-1}, 328 cm^{-1}, 592 cm^{-1}, and at 616 cm^{-1} highlighting well matched findings with the existing literature. Lastly, RAMAN spectrum of ZnO nanoparticles is configured to explain the RAMAN modes of ZnO-based nanoparticles. Conferring to the group theory, optical phonon has eight sets of zone center, in which the modes A1 and E1 exhibits polar behavior which split into transverse optical (A1T and E1T) and longitudinal-optical (A1L and E1L) phonons. Whereas, on the other hand the E2 mode comprises two modes of low- and high-frequency phonons (E2L and E2H). The broad hump known as RAMAN active optical phonon mode showing the ZnO wurtzite hexagonal phase characteristic was detected at 437 cm^{-1}. There also remain few other peaks observant in the spectrum of ZnO-based nanoparticles indicating the presence of pure wrutzite structure ZnO.

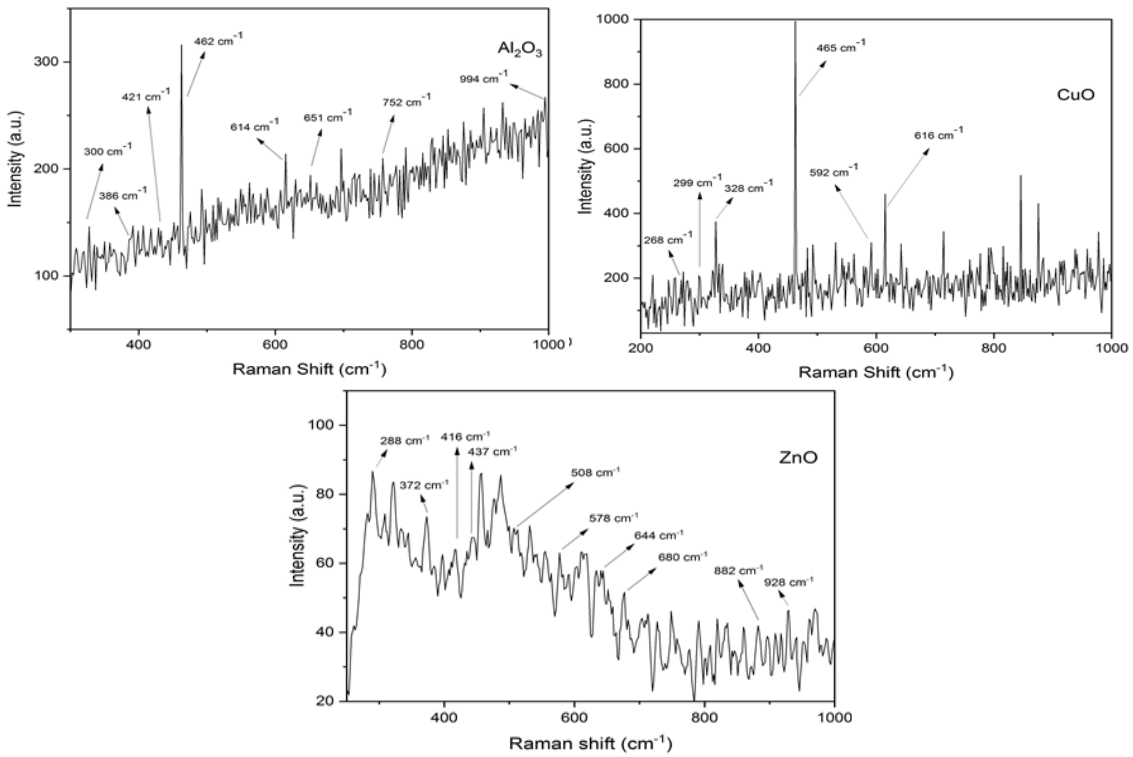

Fig. 3. RAMAN spectroscopy analysis of the synthesized nanomaterials.

3.2. Simulation-based evaluation

The energy band gap of these materials shows that the ZnO has lower band gap than other considered dielectric materials (Figure 4). The density of the states of ZnO-based nanomaterial reveals that the most of the unoccupied electrons reside at lower energy states while comparing with the dielectric nanomaterials such as Al_2O_3 and CuO (Figure 5). The dielectric material energy absorption by electric field was also observed. It was found that the energy absorption maximizes due to the reduction in the band gap. This energy is absorbed due to the alignment of nanoparticles domain walls in the direction of the applied electric field. The dielectric constant for Al_2O_3, CuO and ZnO was measured at lower frequency such as, 1.2×10^4 F/m, 2.4×10^4 F/m and 8×10^4 F/m,

respectively (Figure 6). It is anticipated that the high energy absorption for ZnO-based nanomaterial takes place due to the high dielectric constant, as compared to the Al_2O_3 and CuO. This realization can increase the dielectrophoretic force which then helps to reduce the fluid mobility.

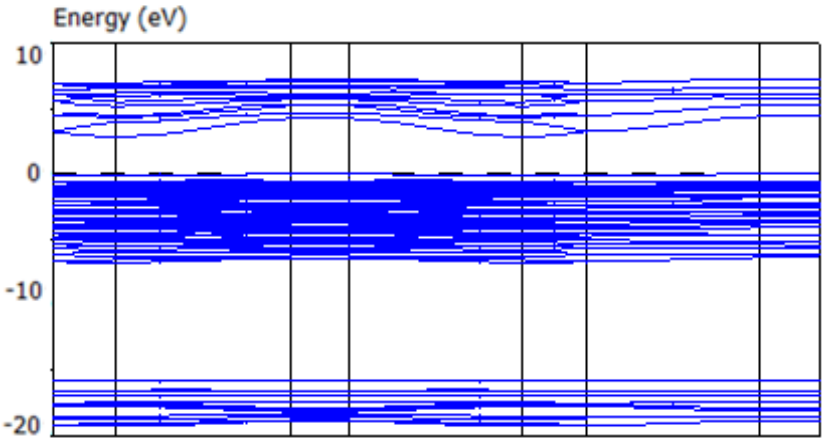

Fig. 4 (a). Energy band gap for Al_2O_3-based nano-material.

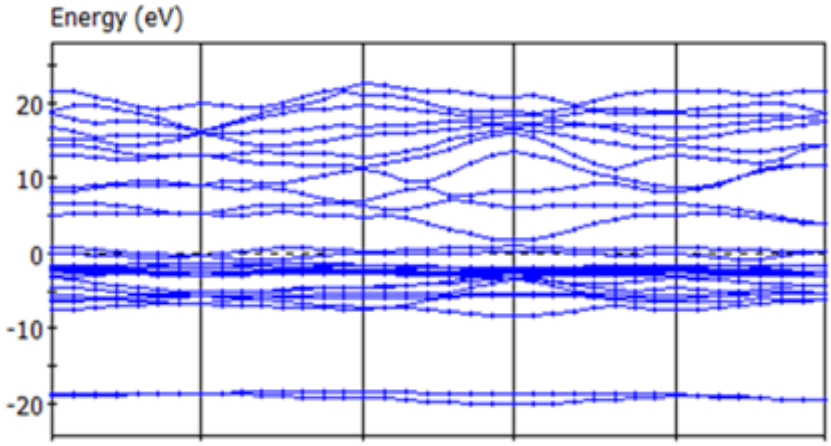

Fig. 4 (b). Energy band gap for CuO-based nano-material.

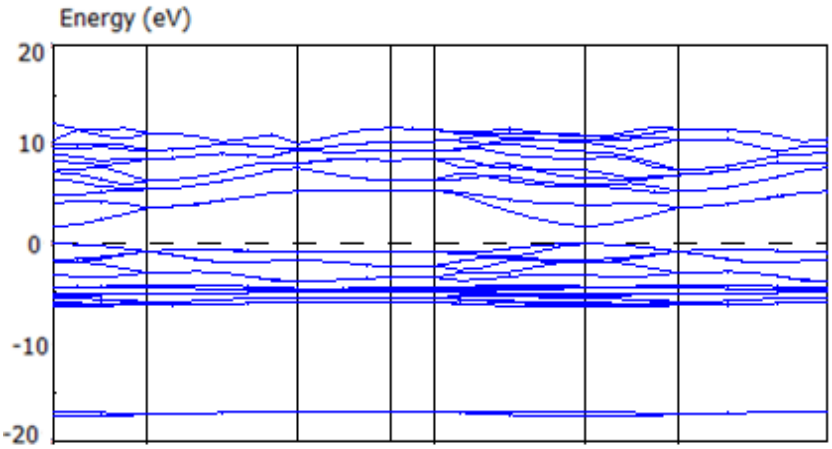

Fig. 4 (c). Energy band gap for ZnO-based nano-material.

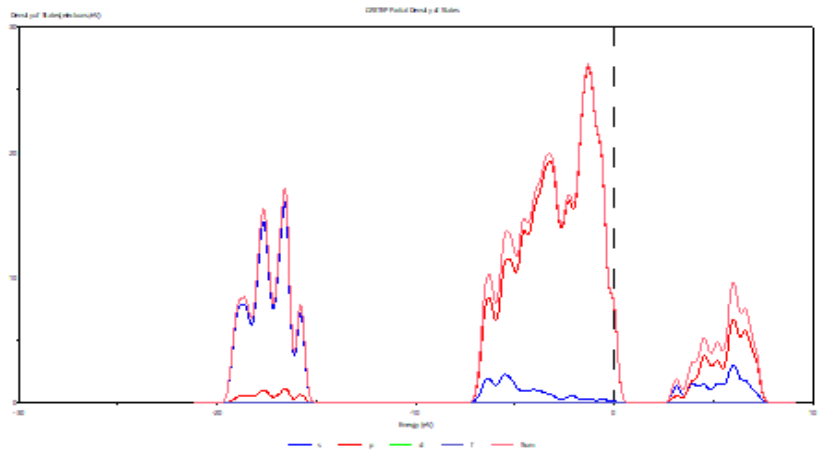

Fig. 5 (a). Projected density of state for Al_2O_3-based nano-material.

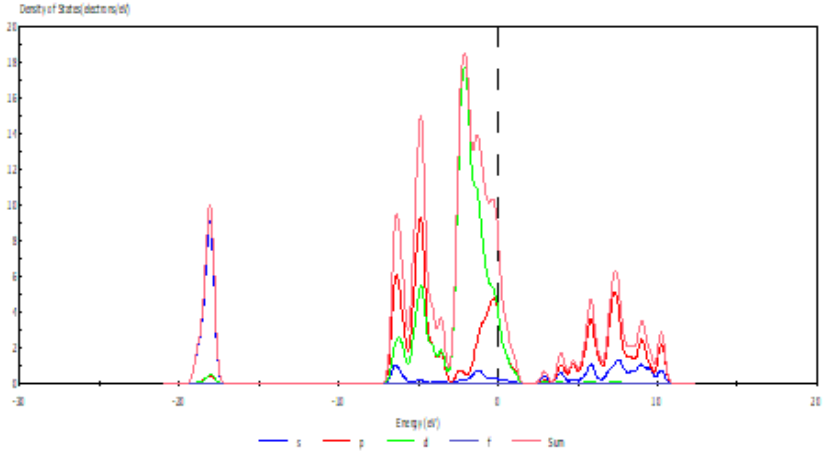

Fig. 5 (b). Projected density of state for CuO-based nano-material.

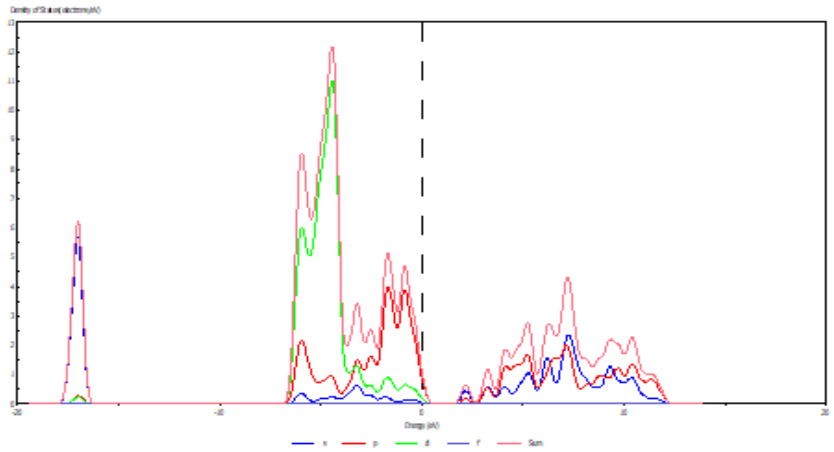

Fig. 5 (c). Projected density of state for ZnO-based nano-material.

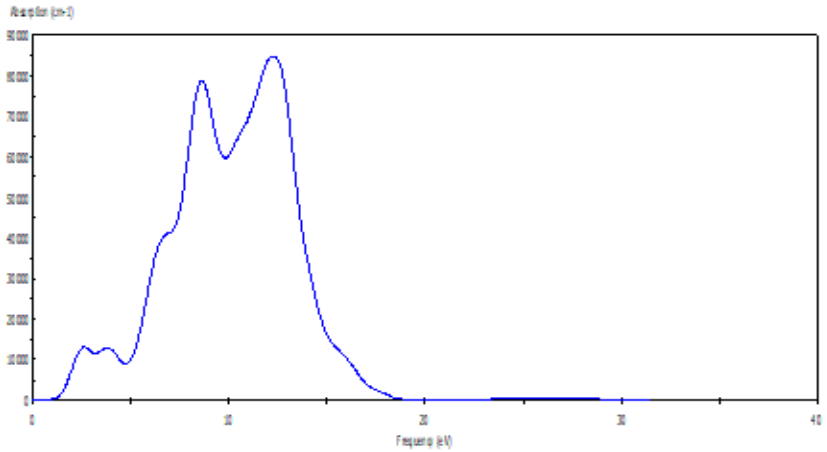

Fig. 6 (a). Dielectric constant for Al_2O_3-based nano-material.

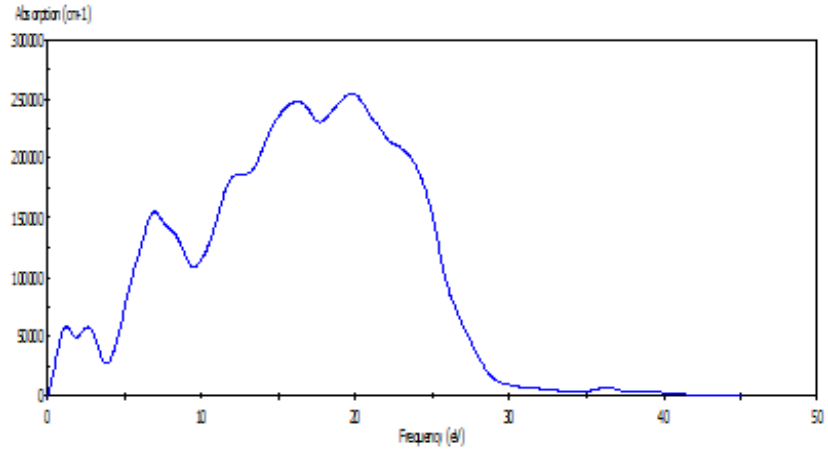

Fig. 6 (b) Dielectric constant for CuO-based nano-material.

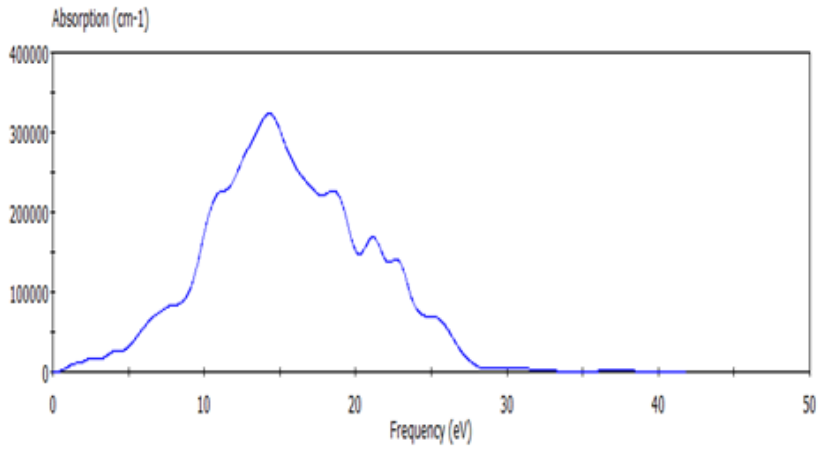

Fig. 6 (c). Dielectric constant for ZnO-based nano-material.

4. Discussion

The IFT behaviour is assessed by placing crude oil with the considered nanofluids based on Al_2O_3, CuO and ZnO. The outcomes are comprehended in table 1. The droplet phase was set to be crude oil whereas the external phase remained brine followed by the nanofluid with and without the

exposure of electromagnetic wave. The addition of nanofluid generated decrement in the IFT to the varying level with respect to different nanofluids. For example, the addition of Al_2O_3 instigated a decrease of IFT by 5.08% when electromagnetic wave exposure was maintained. On the otherhand, a decrement of 7.27% of IFT value on average is witnessed in the presence of CuO nanoparticles. Whereas, the use of ZnO nanofluid facilitated the decrease of 11.3% in the presence of EM wave. The findings seal the utility of ZnO-based nanofluid in the decrease of IFT as compared to the rival nanofluids. Relative enzyme activity which shows how the presence of nanoparticles affects an enzyme's function, is typically calculated by comparing the enzyme's activity in the presence of nanoparticles with its activity in a control sample (without nanoparticles). The formula is: Relative Enzyme Activity (%) = (Enzyme Activity with Nanoparticles/ Enzyme activity in control)*100.

Table 1. IFT measurements for preconsidered settings.

Nanoparticles	Time	Oil + Brine IFT	Oil + Brine + nanofluid IFT (without EM wave)	Oil + Brine + nanofluid IFT (with EM wave)	Relative Enzyme Activity (%)
Al_2O_3	300	24.8	23.8	22.8	98
	400	24.2	23.2	22.5	96
	500	24.0	23.0	22.0	94
	600	23.5	22.8	21.8	92
CuO	300	24.0	22.0	18.2	92
	400	24.5	21.0	17.5	89
	500	23.0	20.0	17.0	87
	600	22.0	19.0	16.8	85
ZnO	300	24.0	20.0	15.0	85
	400	23.5	19.5	13.0	80
	500	22.0	19.0	11.5	78
	600	21.0	18.5	10.0	75

Response Surface Methods were launched to attain the optimal structure. The elaborative scheme is persuaded to investigate the relationships while considering various settings of Temperature, Viscosity, and types of nanofluid as input variables and IFT measurements to determine the optimum response. The residual plots given in figure 7 project the legitimacy of employed strategy.

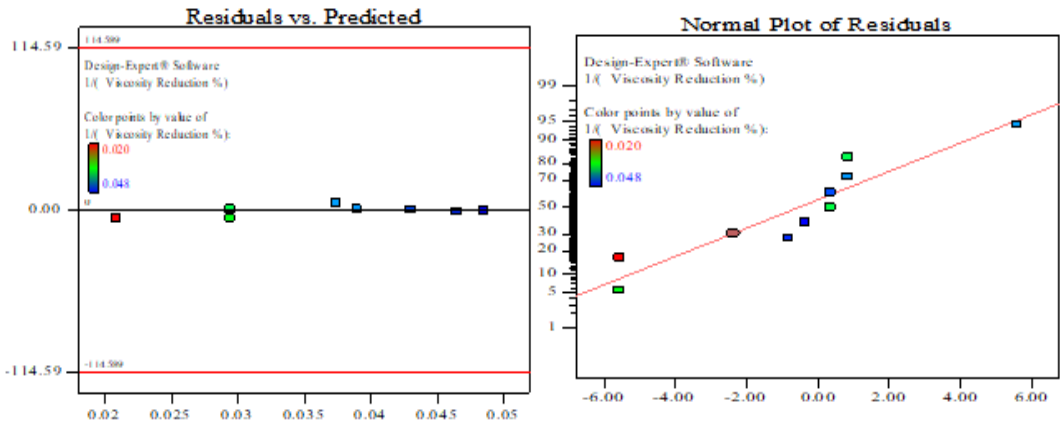

Fig. 7. Residual plots resulting from RSM scheme.

The variability analysis was facilitated by the launch of Analysis of Variance (ANOVA) technique. Table 2 comprehends the results of ANOVA while highlighting the statistical significance of different delicacies involved in the system. One may notice that the overall modelling scheme remains significant with the associated p-value of 0.0333. Further, the significance of nanoparticles is observed while effecting the IFT values in linear fashion with related. Moreover, the temperature is witnessed to be influencing the IFT measurements through quadratic functional.

Table 2. Analysis of variance to optimize the IFT response.

Source of Variation	d.f.	F-Ratio	P-value
Model	6	29.34	0.0333
Temperature	1	6.82	0.1207
Nanoparticles	2	26.94	0.0358
Interaction	2	18.91	0.0502
Temperature^2	1	77.52	0.0127
Residual	2	29.34	0.0333

5. Conclusions

The propensity of IFT reduction was investigated using dielectric nanoparticles with electromagnetic waves. The synthesis of dielectric nanoparticles such as, Al_2O_3, CuO and ZnO was successfully met by the launch of sol gel method. The characters of thus prepared nanoparticles were explored rigorously through the consideration of relevant characterizations and testing. The XRD analysis of Al_2O_3, CuO and ZnO showed that the average crystallite size of pre-considered nanoparticles remained at 43.95 nm, 36.92 nm and 25.2 nm, respectively. Further, morphological attributes were deducted through SEM analysis.

The SEM images revealed that the Al_2O_3 have grain sizes in the range of 66.78 nm to 127.7 nm whereas, for CuO and ZnO it was observed to vary from 63.47 nm to 82.35 nm and from 31.34 nm to 54.01 nm, respectively. Furthermore, agglomeration of nanoparticles was observed which is anticipated to be the result of the togetherness of powder sample stuck due to the effect of surface tension. Moreover, dielectric properties of the prepared nanoparticles were investigated within the frequency range of 40 Hz-25 MHz. It was found that the dielectric constant resulted as 1.58×10^2 F/m, 1.1987×10^4 F/m, 3.5×10^4 F/m, for Al_2O_3, CuO and ZnO, respectively. The findings substantiated that ZnO depicts high dielectric constant at low frequency.

Furthermore, the interfacial tension between the crude oil and nanofluid shows a decrement of 5.08%, 7.27%, and 11.3%, for Al_2O_3, CuO and ZnO, respectively. The modelling-based encapsulation of the system assessed the significance of linear relationship prevalent between IFT readings and materials used in nanoparticles fabrication. Also, quadratic functional relationship was estimated between IFT measurements and temperature. In conclusion, ZnO-based nanofluid was found to be standing out in the providence of more convincing features facilitating the fluid recovery.

References

[1] U. K. Ehigiamusoe, E. Dogan, Renewable and Sustainable Energy Reviews, 154, 111883 (2022); https://doi.org/10.1016/j.rser.2021.111883

[2] N. Gartland, J. Pruyn, Frontiers in Energy Research, 10, 894555 (2022); https://doi.org/10.3389/fenrg.2022.894555

[3] P. Kumawat, Doctoral dissertation, School of Petroleum Management, (2022).

[4] M. Govarthanan, S. Manikandan, R. Subbaiya, Y. R. Krishnan, S. Srinivasan, N. Karmegam, W. Kim, Fuel, 312, 122928 (2022); https://doi.org/10.1016/j.fuel.2021.122928

[5] W. K. Shah, J. P. Ong, H. M. Chua, G. H. S. Toh, C. J. J. Lee, D. Y. X. Soo, Q. Zhu, Energy and Buildings, 112018 (2022); https://doi.org/10.1016/j.enbuild.2022.112018

[6] A. Kamkar, Hosseini, H., S. Norouzi-Apourvari, M. Schaffie, Arabian Journal for Science and Engineering, 47(9), 11609-11622 (2022); https://doi.org/10.1007/s13369-021-06356-2

[7] W. Zhang, Y. Wang, S. Wang, Z. Guo, C. Zhang, X. Zhu, G. Zhang, Journal of Molecular Liquids, 355, 118937 (2022); https://doi.org/10.1016/j.molliq.2022.118937

[8] B. Soerya, J. Edianta, S. Lailaturofi'ah, A. Ningtyas, S. F. Arsyad, D. Setiabudidaya, S. Sailah, Indonesian Physical Review, 5(1), 36-56. (2022); https://doi.org/10.29303/ipr.v5i1.131

[9] O. Tavakkoli, H. Kamyab, M. Shariati, M. A. Mohamed, R. Junin Fuel, 312, 122867, (2022); https://doi.org/10.1016/j.fuel.2021.122867

[10] F. Yakasai, Z. M. Jaafar, S. Bandyopadhyay, A. Agi, A. M. Sidek, Journal of Petroleum Science and Engineering, 208, 109438 (2022); https://doi.org/10.1016/j.petrol.2021.109438

[11] P. M. Yutkin, J. C. Radke, W. T. Patzek, Transport in Porous Media, 141(2), 255-278 (2022); https://doi.org/10.1007/s11242-021-01715-x

[12] G. Yang, Y. Bai, Y. Song, M. S. A. Metwally, O. Mahmoud, Scientific Reports, 12(1), 1-8 (2022); https://doi.org/10.1038/s41598-022-13639-7

[13] M. Takeda, M. Manaka, D. Ito, Journal of Petroleum Science and Engineering, 110731 (2022); https://doi.org/10.1016/j.petrol.2022.110731

[14] Y. Nan, W. Li, Z. Jin, Langmuir, 38(16), 4802-4811 (2022); https://doi.org/10.1021/acs.langmuir.1c03040

[15] M. P. Rendel, B. Mountain, L. K. Feilberg, Journal of Petroleum Science and Engineering, 214, 110484 (2022); https://doi.org/10.1016/j.petrol.2022.110484

[16] W. Tang, P. Wu, C. Da, S. Alzobaidi, J. Harris, B. Hallaman, P. K. Johnston, Fuel, 331, 125752 (2023); https://doi.org/10.1016/j.fuel.2022.125752

[17]. S. Varshney, A. Nigam, J. S. Pawar, N. Mishra, Phosphorus, Sulfur, and Silicon and the Related Elements, 197(2), 72-88 (2022); https://doi.org/10.1080/10426507.2021.2017434

[18]. C. Chua, Y. C. Kee, K. L. Ang, S. Y. Ang arXiv preprint arXiv:2203.00583 (2022).

[19] A. J. Spencer, L. A. Mock, G. A. Jacobs, M. Schubert, Y. Zhang, J. M. Tadjer, Applied Physics Reviews, 9(1), 011315 (2022); https://doi.org/10.1063/5.0078037

[20] J. Zhu, S. S. Araya, X. Cui, K. S. Kær, International Journal of Hydrogen Energy, 47(14), 8700-8715 (2022); https://doi.org/10.1016/j.ijhydene.2021.12.223

[21] X. Guo, F. Liu, Y. Hua, H. Xue, J. Yu, D. Mao, T. F. Ng, Catalysis Today, (2022); https://doi.org/10.1016/j.cattod.2022.02.004

[22]. S. Dehghanpoor, H. M. Sedaghat, A. Bakhtyari, A. M. Makarem, R. M. Rahimpour, Topics in Catalysis, 1-11 (2022); https://doi.org/10.1007/s11244-022-01570-0

[23] A. Sarhan, M. A. Abdelghany, F. El-Dossoki, Egyptian Journal of Chemistry, 65(7), 275-279 (2022).

[24]. Y. Wang, Y. Zhang, T. Wu, W. Fang, X. Kou, T. Wu, J. Kim, Materials Sciences and Applications, 13(9), 491-505 (2022); https://doi.org/10.4236/msa.2022.139030

[25] S. Kinnunen, T. Sajavaara, Surface and Coatings Technology, 441, 128456 (2022); https://doi.org/10.1016/j.surfcoat.2022.128456

[26] G. Prashar, H. Vasudev, Materials Today: Proceedings, 50, 607-611 (2022); https://doi.org/10.1016/j.matpr.2021.03.090

[27]. R. Zhao, Q. Fan, R. Yang, Y. Song, X. Yu, S. Yun, Available at SSRN 4132126. Exploration of Stable Novel Al2o3 by High-Throughput Calculation Screening and Density Functional Theory.

[28] M. Zamen, M. Kahani, B. Rostami, M. Bargahi, Energy Science & Engineering (2022); https://doi.org/10.1002/ese3.1067

[29] B. Ma, X. Ren, Z. Gao, J. Tian, Z. Jiang, W. Zan, G. Fu, International Journal of Applied Ceramic Technology, 19(3), 1265-1273 (2022); https://doi.org/10.1111/ijac.13934

[30] M. Meshksar, F. Salahi, F. Zarei-Jelyani, R. M. Rahimpour, M. Farsi, Journal of Industrial and Engineering Chemistry (2022); https://doi.org/10.1016/j.jiec.2022.04.013

[31]. M. Chandrasekar, M. Subash, S. Logambal, G. Udhayakumar, R. Uthrakumar, C. Inmozhi, K. Kanimozhi, Journal of King Saud University-Science, 34(3), 101831 (2022); https://doi.org/10.1016/j.jksus.2022.101831

[32] N. H. Cuong, S. Pansambal, S. Ghotekar, R. Oza, T. T. N. Hai, M. N. Viet, H. V. Nguyen, Environmental Research, 203, 111858 (2022); https://doi.org/10.1016/j.envres.2021.111858

[33] Y. Gao, W. Yuling, International Journal of Biological Macromolecules, (2022); https://doi.org/10.1016/j.ijbiomac.2022.01.162

[34]. E. B. Al-Jumaili, Optical Materials, 133, 112897 (2022); https://doi.org/10.1016/j.optmat.2022.112897

[35] I. S. Kunya, Y. Abdu, K. M. Mustafa, K. M. Ahmad, Journal of Chemistry Studies, 1(2), 17-26 (2022); https://doi.org/10.32996/jcs.2022.1.2.3

[36]. T. M. Noman, N. Amor, M. Petru, Critical Reviews in Solid State and Materials Sciences, 47(2), 99-141 (2022); https://doi.org/10.1080/10408436.2021.1886041

[37] A. A. Mutalib, F. N. Jaafar, Total Environment Research Themes, 100013 (2022); https://doi.org/10.1016/j.totert.2022.100013

[38] R. Sha, A. Basak, C. P. Maity, S. Badhulika, Sensors and Actuators Reports, 100098 (2022); https://doi.org/10.1016/j.snr.2022.100098